

Charge Separation and Charge Transfer in the Low-Lying Excited States of Pentacene

Published as part of *The Journal of Physical Chemistry virtual special issue "Josef Michl Festschrift"*.

Bushra Alam, Adrian F. Morrison, and John M. Herbert*

Cite This: *J. Phys. Chem. C* 2020, 124, 24653–24666

Read Online

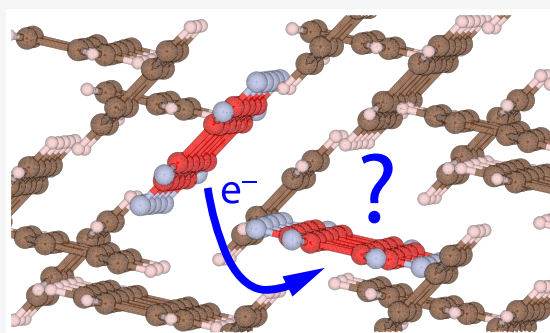
ACCESS |

Metrics & More

Article Recommendations

Supporting Information

ABSTRACT: Pentacene thin films are common constituents of organic photovoltaic materials and a prototypical example of a material that undergoes singlet exciton fission, but significant questions remain regarding the mechanism. In particular, theoretical studies have reached differing conclusions regarding the role (and even the presence) of low-energy charge-transfer (CT) states in this material. Periodic electronic structure calculations predict low-energy CT states in crystalline pentacene but correlated wave function calculations on cluster models (typically dimers) have generally failed to find evidence of CT states at energies relevant to singlet fission. Here, we use an *ab initio* exciton model to examine size-dependent trends in low-energy CT states, in models ranging from pentacene dimer to hexamer. We complement these results with additional calculations using time-dependent density functional theory. Our calculations support the idea that dielectric stabilization leads to the appearance of low-energy CT states in the crystalline material that are absent in dimer models, but which (in larger models) become accessible at photon energies relevant to singlet fission. Optimally-tuned and screened range-separated hybrid functionals, which set the frontier orbital energies in a nonempirical way, predict a greater degree of charge separation as compared to other common range-separated hybrid functionals. We examine electron–hole correlations in these calculations, which reveal underlying charge separation in the excited states that may go undetected by other qualitative analysis tools. These results help to connect dimer quantum chemistry to periodic calculations, and they suggest that the former are inadequate models for singlet fission.



1. INTRODUCTION

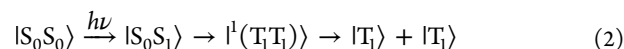
Singlet fission (SF) is the spin-allowed formation of two triplets from the single-photon excitation of a state with singlet multiplicity, i.e., multiple exciton generation.^{1,2} It is observed most commonly in π -conjugated chromophores and is of interest in organic photovoltaic (OPV) applications, where it holds the potential to amplify solar cell efficiencies beyond the Shockley–Queisser or detailed balance limit.^{3–5} SF has been reported for a large number of chromophores, but its mechanism continues to be debated.^{6–10}

SF is expected to be most efficient when the energy of the excited singlet state (S_1) is at least twice the energy of the triplet state:

$$E(S_1) \geq 2E(T_1) \quad (1)$$

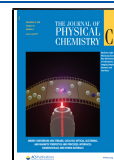
This is indeed the case for pentacene, which is the archetypal SF material and for which SF is exothermic by 0.1–0.2 eV.^{11,12} In crystalline tetracene, however, $2E(T_1)$ exceeds $E(S_1)$ by 0.18–0.20 eV.^{13,14} Despite this, SF is observed to be fast and efficient in both materials, with a rate that is independent of temperature.^{3,15} This has led to much debate about the role of vibronic coherence in promoting endothermic SF in tetracene.^{6,16–18}

Even for the exothermic case in pentacene, the SF mechanism remains unclear. It is commonly represented as a two-step process,^{1,2}



that proceeds via an intermediate “triplet-pair” or “multiexciton” (ME) state $|^1(T_1T_1)\rangle$, which consists of triplet states on two different pentacene monomers whose spins are entangled and coupled to an overall singlet. (A role for a quintet ME state, $|^5(T_1T_1)\rangle$, has also been suggested in intramolecular SF.¹⁹) Ultimately, the entangled multiexciton suffers dephasing and diffuses apart to form triplet charge carriers $|T_1\rangle$ on two different monomers, as indicated in eq 2 and also in Figure 1, which illustrates several proposed mechanisms for SF. One proposal is a direct-coupling

Received: August 31, 2020
Revised: October 8, 2020
Published: October 28, 2020



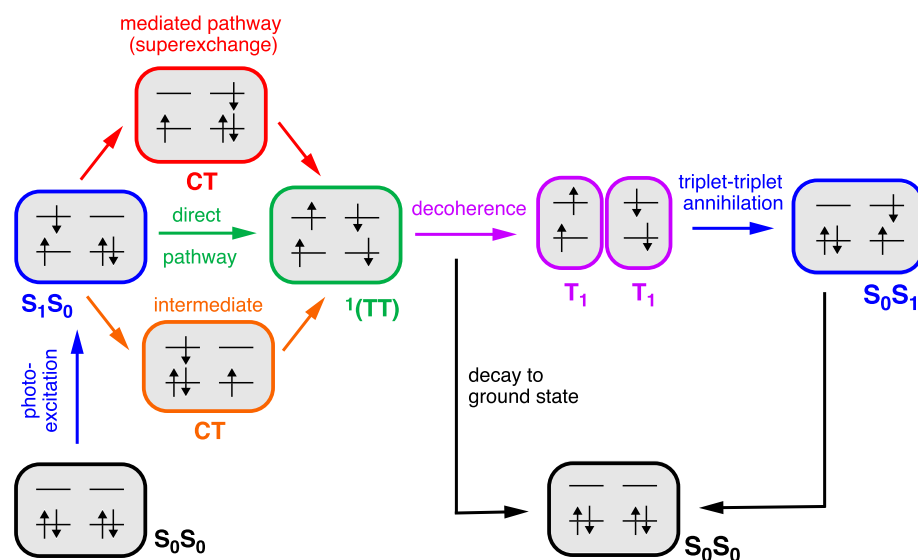


Figure 1. Schematic view of proposed mechanisms for SF. The initial photoexcited state is depicted as $|S_0S_1\rangle$ here, although it could be a Frenkel exciton mixture of $|S_0S_1\rangle$ and $|S_1S_0\rangle$, as in eq 4. Several proposed mechanisms for subsequent generation of the triplet-pair state are illustrated. The direct-coupling mechanism posits excitation energy transfer directly between $|S_0S_1\rangle$ and $|^1(T_1T_1)\rangle$, without the need to invoke other states. Mechanisms involving CT states, which could appear in charge-resonance pairs (eq 3), include a superexchange mechanism involving higher-energy CT states or alternatively a CT-mediated mechanism wherein these states are low enough in energy to serve as proper intermediates.

mechanism in which the $|^1(T_1T_1)\rangle$ state is populated directly by excitation energy transfer from the initially prepared S_1 state.⁸

Two other possible mechanisms for SF invoke charge-transfer (CT) states. These are not explicated in eq 2 but have been suggested to participate in a mediated mechanism.^{6,20–22} These states are often denoted $|^1(AC)\rangle$ (for “anion–cation”) and $|^1(CA)\rangle$,² although for high-symmetry dimers they may show up as linear combinations

$$|CR\rangle = a_1|^1(AC)\rangle + a_2|^1(CA)\rangle \quad (3)$$

that are known as charge-resonance states. Analogously, the initially excited state may not be strictly $|S_0S_1\rangle$ but rather the Frenkel exciton state

$$|FE\rangle = b_1|S_0S_1\rangle + b_2|S_1S_0\rangle \quad (4)$$

with equal coefficients $b_1 = b_2$ in the limit of a symmetric dimer. Studies on crystalline tetracene suggest that the lowest bright state is delocalized over ≈ 7 monomers.²³

The role of charge-separated states in SF remains a matter of debate. A two-step, CT-mediated mechanism has been invoked to explain coherent beats observed in time-resolved experiments,^{20,22} and has been implicated in intramolecular SF as well.²⁴ According to this proposal, the coherences result from a superposition state consisting of $|FE\rangle$, $|^1(T_1T_1)\rangle$, and the CT states.²¹ It has been argued that couplings between the Frenkel exciton state and the ME state, which are estimated to be 0.5–3.0 meV for tetracene, are not large enough to account for the ultrafast formation of the ME state via a direct-coupling mechanism, and thus direct coupling cannot explain the results of time-resolved two-photon photoemission spectroscopy.⁶ Couplings between $|FE\rangle$ and the CT states were estimated to be significantly larger (50–140 meV) and this was taken as evidence in favor of the quantum-coherent mechanism.⁶ It bears pointing out, however, that the mere existence of a coherence does not explain the observation of barrierless yet endothermic SF.³

A role for CT states has also been suggested in some theoretical studies based on model Hamiltonians.^{25,26} As indicated in Figure 1, these states need not appear below the bright states in order to participate in SF, but could instead be part of a superexchange mechanism in which higher-energy CT states couple to other relevant states (whose diabatic labels are indicated in eq 2) through higher orders of perturbation theory but are never themselves significantly populated.²⁷ Couplings to CT states have also been introduced into theoretical models in order to reproduce observed Davydov splittings in the absorption spectra of tetracene and pentacene.^{20,28} For pentacene, various other spectroscopies have been interpreted by means of simulations that invoke coupling to CT states.^{10,29,30}

In addition to these phenomenological models there have been numerous attempts to characterize the low-energy excited states of pentacene and other SF materials using electronic structure theory.³¹ These calculations are challenging in part because of the doubly excited nature of the $|^1(T_1T_1)\rangle$ state,^{32,33} which is therefore missing from single-excitation theories including time-dependent density functional theory (TDDFT).^{32,34} The energetics of the $|^1(T_1T_1)\rangle$ state may therefore be unreliable unless highly correlated wave functions are employed. A second complication is the potential role of dielectric stabilization of charge-separated states by the crystalline environment. If one’s goal is to understand the optical spectrum of solid-state pentacene (or even thin films), then large model systems may be required in order to correctly position the CT states in the spectrum.

Pentacene has been studied in a periodic framework using G_0W_0 calculations combined with the Bethe–Salpeter equation, with the conclusion that the low-energy states in the optical spectrum exhibit significant charge separation.^{35–40} (This can be inferred by visualizing electron–hole correlation functions for the excited states in real space.³⁸) The same methodology predicts low-energy CT states already in dimers and trimers of pentacene, in herringbone geometries extracted from the crystal structure of the bulk material.⁴¹ At the

CASPT2 level, a state with significant CT character (as indicated by an excited-state dipole moment of 13 D) emerges as the lowest excited state of the herringbone pentacene dimer,⁴¹ although no such state is reported in other CASPT2 calculations of (pentacene)₂.⁴² Dimer geometries differ between these two calculations, and in addition the CT energy levels were found to be sensitive to the choice of active space.⁴¹ One lesson from the present study is that geometry can make a significant difference in small pentacene cluster models.

The study in ref 41 stands as an outlier in the quantum chemistry literature, whereas a variety of other calculations seem to support the conclusion that there is little if any CT character in the low-lying excited states of either tetracene or pentacene dimer. These include calculations using a restricted active space double spin-flip (RAS-2SF) method,^{23,32,43–45} which does not include much dynamical correlation⁴⁶ but readily incorporates $|^1(T_1T_1)\rangle$ into the excitation space. These RAS-2SF calculations do find CT character in higher-lying excited states but not at energies relevant to SF.⁴³

Especially in dimers, charge-separated states often appear as symmetrized linear combinations (eq 3), which may have small or even vanishing dipole moments, even if the basis states $|^1(AC)\rangle$ and $|^1(CA)\rangle$ have large dipole moments. In addition to the RAS-2SF studies mentioned above, other correlated wave function studies have also concluded that charge-separated configurations have very low weight in the low-lying excited-state wave functions of pentacene dimer.^{47,48}

The present work aims to reconcile these disparate views and observations on the role of low-lying CT states in pentacene, using a systematic approach and some theoretical tools different from those discussed above. In that regard, we employ an *ab initio* exciton model developed previously by two of us,^{17,49–52} which amounts to a form of nonorthogonal configuration interaction in a direct-product basis where the basis states have readily identifiable diabatic character: Frenkel excitons, CT states, and ME states. Rather than investigating the ME states in detail, these calculations are designed to investigate the role, and the positioning in the optical spectrum, of the CT states, and we will complement these calculations with TDDFT calculations using range-separated hybrid (RSH) functionals. A second key aspect of this work is the systematic application of these methods to cluster models of pentacene ranging from dimer to hexamer. By examining the size-dependence of the low-lying excited states, we aim to connect existing dimer quantum chemistry calculations to periodic calculations of crystalline pentacene.

2. COMPUTATIONAL METHODS

All calculations were performed using Q-Chem v. 5.2⁵³ and wave function analysis was carried out using TheoDORE, v. 2.1.⁵⁴ The electronic structure models are described in this section. All calculations use the 6-31+G* basis set.

2.1. Exciton Model. Extracting qualitative (essentially diabatic) information from a multiconfigurational wave function representing an adiabatic electronic state can be a challenge, especially when the chromophores (individual pentacene monomers, in the present case) are closely packed, as in an OPV material. Note, for example, that excited-state wave functions for both the $|ICR\rangle$ state (eq 3) and the $|IFE\rangle$ state (eq 4) of the dimer will be delocalized over both monomers, assuming that the mixing coefficients have comparable magnitude. As such, a conceptually useful approach to extract qualitative information on the nature of

the excited states is nonorthogonal configuration interaction (CI) in a basis of monomer states, to which diabatic labels can be easily assigned. The mixing coefficients, which emerge naturally from solution of Schrödinger's equation, then quantify the extent to which each diabatic basis state participates in a given adiabatic eigenvector. This is the gist of the *ab initio* Frenkel–Davydov exciton model (AIFDEM) introduced previously by two of us.^{17,49–52} This method may be considered a form of renormalization of the CI problem, in which the excitation space for the supersystem can be made rather compact because individual CI problems have already been solved on the monomers.

An alternative point of view on the AIFDEM is historical and is where the name originates. Frenkel defined the exciton to be a superposition of excitation waves, while Davydov proposed a Hamiltonian for molecular crystals that is a sum of single-site and pairwise interaction terms:⁵⁵

$$\hat{H} = \sum_n \hat{H}_n + \sum_{m < n} \hat{V}_{mn} \quad (5)$$

Because the exact (Coulomb) Hamiltonian has a pairwise form, there is no approximation inherent in writing eq 5, although often the term “Frenkel exciton model” is synonymous with a dipole-coupling approximation for \hat{V}_{mn} . Such an approximation is suspect at the closed-packed geometries of molecular crystals, and is not used here. Instead, the AIFDEM diagonalizes the full Coulomb Hamiltonian but in a limited direct-product “exciton-site basis”.⁵⁵ In its present implementation, AIFDEM calculations are limited to single substitutions on one monomer at a time, e.g.,

$$|\Psi_A^* \Psi_B \Psi_C\rangle = |\Psi_A^*\rangle \otimes |\Psi_B\rangle \otimes |\Psi_C\rangle \quad (6)$$

In this example, $|\Psi_B\rangle$ and $|\Psi_C\rangle$ are the ground-state self-consistent field (SCF) wave functions for monomers B and C whereas

$$|\Psi_A^*\rangle = \sum_{ia\sigma} C_{ia\sigma}^A |q_A^{ia}\rangle \quad (7)$$

is a linear combination of singly substituted Slater determinants $|q_A^{ia}\rangle$. Coefficients $C_{ia\sigma}^A$ (where σ is a spin index) are computed by means of a CI-singles (CIS) calculation on monomer A.

Following CIS calculations on each monomer to generate the wave functions $\{|\Psi_A^*\rangle\}$, an AIFDEM calculation proceeds by constructing the full Coulomb Hamiltonian in the nonorthogonal direct-product basis. This is the bottleneck step, requiring a single Fock build per matrix element in the basis set of the full system, but this step is also trivially parallelizable.⁴⁹ Diagonal matrix elements such as $\langle \Psi_A^* \Psi_B \Psi_C | \hat{H} | \Psi_A^* \Psi_B \Psi_C \rangle$ constitute exciton-site energies, and off-diagonal matrix elements such as $\langle \Psi_A^* \Psi_B \Psi_C | \hat{H} | \Psi_A^* \Psi_B^* \Psi_C \rangle$ are energy-transfer couplings. Although the AIFDEM allows these matrix elements to be computed in a fully *ab initio* way, such that the only approximation is the truncated direct-product basis (Frenkel exciton *ansatz* itself), following ref 50 we use charge embedding for any monomer wave functions in the bra and ket that are not directly coupled by \hat{H}_n or \hat{V}_{mn} .

The site basis used in the present study consists of the locally excited (LE) states (one per monomer), CT states, and ME states. For pentacene dimer, this means the four basis states in eqs 3 and 4 plus $|^1(T_1T_1)\rangle$. The latter is constructed

by coupling the monomer triplet wave functions $|\Psi_A^{T_m}\rangle$ and $|\Psi_B^{T_m}\rangle$ ($m = -1, 0, 1$) to an overall singlet:¹⁷

$$\begin{aligned} |\Psi_A^T \Psi_B^T\rangle &= \frac{1}{\sqrt{3}} |\Psi_A^{T_0} \Psi_B^{T_0}\rangle + \frac{1}{\sqrt{3}} |\Psi_A^{T_{-1}} \Psi_B^{T_{-1}}\rangle \\ &\quad - \frac{1}{\sqrt{3}} |\Psi_A^{T_1} \Psi_B^{T_1}\rangle \end{aligned} \quad (8)$$

For a system composed of n pentacene monomers, the exciton-site basis includes the ground state, n LE or Frenkel exciton states, $n(n-1)$ pairwise CT states, and $n(n-1)/2$ triplet-pair states, for a total of $(3n^2 - n + 2)/2$ configurations. Only a single LE state is included per monomer, representing the lowest CIS excited state for each, as the next state is ≈ 2 eV higher in energy. To reduce the cost of the calculations, CIS expansions in eq 7 are transformed to a basis of natural transition orbitals (equivalent to CIS natural orbitals) and the expansion is truncated with a threshold of 50%, consistent with previous work.^{49,50} Diagonalization of the exciton Hamiltonian affords adiabatic excitation energies, and the corresponding eigenvectors are naturally expressed in a diabatic basis that facilitates straightforward identification of CT character, simply by examining the CI coefficients in the exciton-site basis.

2.2. TDDFT. Although convenient for interpretive purposes, the AIFDEM in its present form lacks dynamical electron correlation so we complement these calculations with additional results obtained using linear-response TDDFT in conjunction with a variety of RSH functionals.^{56–58} The deficiencies of generalized gradient approximations (GGAs) for charge-separated states are well documented,^{59–62} but RSH functionals have been used successfully in this context.^{63–69} Range separation of the electron–electron Coulomb potential has the general form

$$\frac{1}{r_{12}} = \frac{1 - [\alpha + \beta \operatorname{erf}(\omega r_{12})]}{r_{12}^{\text{SR}}} + \frac{\alpha + \beta \operatorname{erf}(\omega r_{12})}{r_{12}^{\text{LR}}} \quad (9)$$

with parameters α , β , and ω . The parameter ω controls the separation of r_{12}^{-1} into short-range (SR) and long-range (LR) components whereas α controls the fraction of short-range Hartree–Fock exchange. Semilocal GGA exchange is applied using the SR (attenuated) Coulomb potential, and Hartree–Fock exchange is applied using the LR (background) part.

Given a GGA functional $E_{\text{xc}} = E_{\text{c}}^{\text{GGA}} + E_{\text{x}}^{\text{GGA}}$, its RSH analogue is

$$\begin{aligned} E_{\text{xc}}^{\text{RSH}} &= \alpha E_{\text{x, HF}}^{\text{SR}} + (\alpha + \beta) E_{\text{x, HF}}^{\text{LR}} + (1 - \alpha) E_{\text{x, GGA}}^{\text{SR}} \\ &\quad + (1 - \alpha - \beta) E_{\text{x, GGA}}^{\text{LR}} + E_{\text{c}}^{\text{GGA}} \end{aligned} \quad (10)$$

where

$$E_{\text{x, GGA}}^{\text{LR}} = E_{\text{x}}^{\text{GGA}} - E_{\text{x, GGA}}^{\text{SR}} \quad (11)$$

In keeping with other literature,^{70–72} we designate the difference between a conventional GGA functional and its attenuated counterpart as “LR” exchange (eq 11). This means, for example, the difference between PBE and ω PBE exchange. In truth, however, this is something of a misnomer because semilocal GGA exchange vanishes as density overlap vanishes and is therefore intrinsically short-ranged; this is the reason range separation and long-range corrected functionals were introduced in the first place! For a charge-separated state, only

the nonlocal term $(\alpha + \beta) E_{\text{x, HF}}^{\text{LR}}$ in eq 10 provides any long-distance interaction between electron and hole, and therefore the asymptotic behavior of the electron–hole interaction potential is $\sim (\alpha + \beta)/r$. This is the correct asymptotic distance dependence (in the gas phase) provided that $\alpha + \beta = 1$. For a solid-state organic material, however, the appropriate asymptotic behavior is $\sim (\epsilon r)^{-1}$ where ϵ is the dielectric constant of the material, and thus a screened RSH (sRSH) formalism has been suggested in which the coefficient of long-range Hartree–Fock exchange is set to $1/\epsilon$ (that is, $\alpha + \beta = 1/\epsilon$).⁷⁰ The sRSH approach has been applied successfully to reproduce fundamental gaps and optical absorption spectra of solid-state materials, using nonperiodic calculations.^{71–73}

Some of the density functionals that we will use in this study are popular ones whose range-separation parameters have been empirically determined to minimize statistical errors over various data sets. These include ω B97X-V,⁷⁴ for which $\omega = 0.30$ bohr⁻¹, and CAM-B3LYP with $\omega = 0.33$ bohr⁻¹.⁵⁶ The former is among the best-performing functionals for a wide variety of ground-state properties,⁷⁵ whereas the latter performs reasonably well in TDDFT benchmarks.^{76–78} That said, CAM-B3LYP does sacrifice the correct long-range constraint $\alpha + \beta = 1$, in the interest of reducing errors for localized valence excitation energies.

Excitation energies of OPV materials, as well as the charge separation observed in the states themselves, are known to be sensitive to the choice of range separation.^{66,79–82} In addition to the aforementioned functionals we will therefore examine results using RSH and sRSH functionals that employ an “optimally tuned” (OT) value of ω .^{64,66} The precise value is determined by minimizing the quantity

$$J(\omega) = [\epsilon_{\text{HOMO}}(\omega) + \text{IE}(\omega)]^2 + [\epsilon_{\text{LUMO}}(\omega) + \text{EA}(\omega)]^2 \quad (12)$$

involving the ionization energy (IE) and the electron affinity (EA) of the system in question. The quantities ϵ_{HOMO} and ϵ_{LUMO} are the frontier orbital eigenvalues. Minimization of $J(\omega)$ represents an attempt to enforce the criterion

$$\text{IE} = -\epsilon_{\text{HOMO}} \quad (13)$$

for both the molecule and its anion. (Equation 13 is a theorem in exact DFT.⁸³) By way of nomenclature, we refer to these tuned functionals as, e.g., OT-RSH- ω PBE if the original functional is LRC- ω PBE, a functional that is described in refs 58 and 84. We will also use OT functionals based on LRC- μ BLYP^{57,65} and LRC- ω PBeh.⁵⁸ See eqs S1–S6 for explicit definitions of these functionals.

The use of OT-sRSH functionals in the presence of a polarizable continuum model (PCM),⁸⁵ which also uses the dielectric constant of the crystal, has been shown to be effective in reproducing fundamental gaps of bulk crystalline materials using nonperiodic calculations.⁷² We use this framework to calculate excitation energies for (pentacene)₆, with the OT-sRSH- ω PBE functional and a PCM environment, in order to estimate the magnitude of the changes expected in transitioning to bulk dielectric stabilization. In an effort to capture the effects of electronic polarization upon vertical excitation, we use a nonequilibrium PCM formalism^{86–88} that separates the “fast” (electronic) component of the polarization from the “slow” (orientational) component, the latter of which is frozen for a vertical excitation process and should not be present in a crystalline environment anyway.

3. RESULTS AND DISCUSSION

3.1. Exciton Model. We examine the $(\text{pentacene})_n$ clusters that are shown in Figure 2. These were extracted from the crystal structure of solid pentacene and were not relaxed, in order to preserve the crystalline spacing between the monomers. The herringbone dimer (Figure 2a) is a widely studied model system but we also consider a hexamer and two tetramers. Of the latter, one has four monomer units arranged in an extended or linear fashion (Figure 2b) whereas the other tetramer is more compact (Figure 2c).

The nature of each AIFDEM eigenstate can be readily inferred by examining CI coefficients in the exciton-site basis, and as an example the AIFDEM eigenvectors for pentacene dimer are listed explicitly in Table 1. Examination of the CI coefficients allows us to assign diabatic labels to these states: single-exciton (SE), ME, and CT. It is immediately obvious that the lowest excited states have the largest coefficients corresponding to CT basis states. That being the case, it is perhaps then not surprising that the lowest-lying states in the larger pentacene clusters are also CT states. AIFDEM excitation energies for the four different clusters examined here plotted in Figure 3.

The tetramer and hexamer excitation spectra are examined in detail in Figure 3a and Figure 3b, respectively, where we have partitioned the excitation spectra into “CT states” and “non-CT states” according to the dominant coefficient in each CI vector. These are qualitative labels and it is important to note that the diabatic basis states do mix in the excitonic eigenstates; the important message to take away from this analysis is that states with substantial CT character do exist at low excitation energies.

This preponderance of CT states in the low-energy part of the spectrum stands in sharp contrast to most other *ab initio* studies of pentacene (and tetracene) dimers, for which CT states are found either to be too high in energy to be of relevance for SF,^{32,43} or else the amount of CT character in the low-energy states was considered negligible.^{8,47,48} In contrast, the low-energy spectrum predicted by the AIFDEM is dominated by CT states, in agreement with theoretical studies of crystalline pentacene suggesting that the lowest-energy excitations in the optical spectrum are CT states.^{36–40} Other

theoretical studies of crystalline pentacene have invoked CT states to explain the origin and magnitude of Davydov splittings,^{20,25,37} featured such states in calculations of the absorption spectrum,^{25,37–39} and used CT states in calculations of the SF rate to account for ultrafast formation of the ME state.^{25–27}

Our pentacene dimer structure (Figure 2a) constitutes the unit cell of the crystal, and by applying the AIFDEM to supercells of increasing size we can begin to mimic the dielectric stabilization of the crystalline environment, yet in a manner that can be connected back to results for the gas-phase dimer that has been the subject of numerous quantum chemistry studies. Figure 3c plots the excitation spectra of all four clusters together, and it is clear that the larger systems stabilize all of the states, including the CT states, and that the CT states are better stabilized in the compact tetramer as compared to the linear one. The change in geometry affects the CT states much more so than the non-CT states, and this geometry dependence ought to be considered carefully in any finite cluster model of an OPV material. Broadly speaking, these observations represent the cluster analogue of dielectric stabilization in the crystal, which is expected but has not been hitherto observed in quantum chemistry studies based on correlated wave functions, due to restrictions on system size. Those restrictions are mitigated in the present work by the inherently parallelizable nature of the exciton model.

A different point of view is obtained if the excitation energies of all four systems are plotted together, not as a function of excitation energy (as in Figure 3c) but rather grouping together states of similar diabatic character. Such a representation is shown in Figure 4, where the states are grouped into SE, ME, and CT states. The latter categories experience relatively larger stabilization as the system size is increased. For example, the lowest-energy CT state drops by 1.3–1.8 eV between the dimer and hexamer structures, as compared to a 1.7 eV decrease for the ME states and only 1.0 eV for the SE states. Thus, the CT states depend on system size in quite a different way than the bright SE states, and we believe this size-dependent trend should continue out to bulk dielectric stabilization. In principle, this extrapolation to the bulk material could be accelerated using continuum boundary conditions, but these are not yet implemented for the AIFDEM. We will consider continuum boundary conditions for the TDDFT calculations that are reported in the next section.

3.2. TDDFT Excitation Energies and Dipole Moments.

To study the excitation spectrum of pentacene at a correlated level of theory we turn to TDDFT. A variety of RSH functionals were tuned using the $J(\omega)$ metric of eq 12 and the tuned values of ω are listed in Table S1. These OT-RSH range separation parameters range from $\omega = 0.195$ – 0.210 bohr⁻¹, which is significantly smaller than values obtained from empirical parametrization of RSH functionals, which are typically 0.30–0.47 bohr⁻¹.^{58,84,89,90} This immediately suggests that one should expect a difference between properties computed using OT-RSH functionals and those obtained using empirically parameterized functionals. We also notice that tuned values of ω are smaller when the base functional is a hybrid (e.g., PBEh rather than PBE), and thus when the RSH functional contains short-range Hartree–Fock exchange. This has been observed also when the range-separation parameter is optimized empirically using experimental data, e.g., where a value $\omega = 0.2$ bohr⁻¹ is optimized for LRC- ω PBEh,³⁸ versus ω

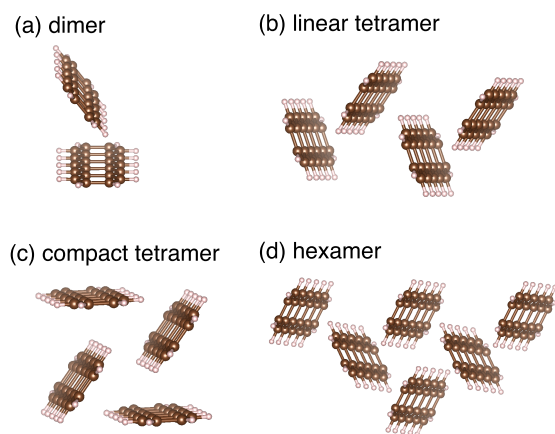


Figure 2. Pentacene clusters included in this study: (a) dimer, which is also the unit cell of crystalline pentacene; (b) tetramer in a linear arrangement; (c) tetramer in a compact arrangement; and (d) hexamer. Each structure was extracted from the crystal structure of solid pentacene and has not been relaxed.

Table 1. AIFDEM Eigenvectors for (Pentacene)₂ in the Exciton-Site Basis^a

exc. energy (eV)	S ₀ ⟩	CT ₁ ⟩	CT ₂ ⟩	SE ₁ ⟩	ME⟩	SE ₂ ⟩
		2.05	2.78	3.59	3.77	3.80
Ψ _A ⁺ Ψ _B ⟩	0.997	0.034	-0.032	0.054	-0.006	0.027
Ψ _A [*] Ψ _B ⟩	-0.032	0.026	0.045	0.062	-0.127	1.012
Ψ _A ⁻ Ψ _B ⟩	-0.056	-0.035	-0.111	1.014	-0.005	-0.059
Ψ _A ⁺ Ψ _B ⁻ ⟩	-0.020	-0.006	-0.991	-0.117	-0.033	0.052
Ψ _A ⁻ Ψ _B ⁺ ⟩	-0.029	0.993	-0.009	0.034	-0.096	-0.047
¹ (TT)⟩	-0.002	0.093	-0.029	0.013	1.103	0.136

^aLargest coefficient for each eigenvector is highlighted in bold. Note that the basis states are nonorthogonal.

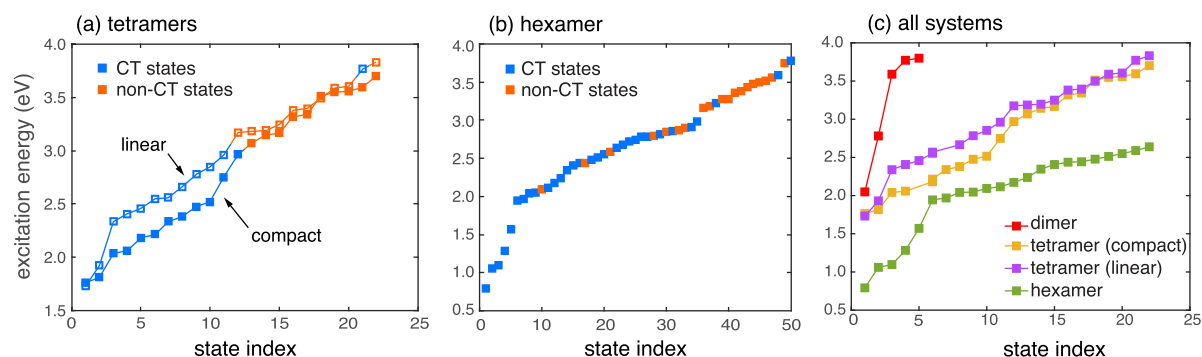


Figure 3. AIFDEM excitation energies for pentacene clusters: (a) the first 25 excited states of the linear tetramer (open symbols) and the compact tetramer (filled symbols); (b) the first 50 excited states of (pentacene)₆; (c) the dimer, tetramer, and hexamer excited states plotted together. In parts a and b, each state is categorized as either CT-like or not according to the largest coefficient in the CI vector, expressed in the exciton-site basis.

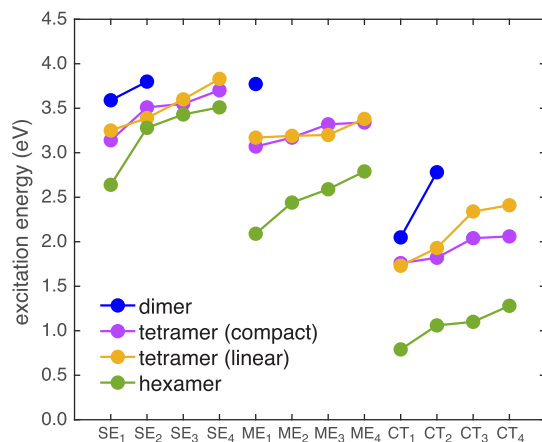


Figure 4. AIFDEM excitation spectra for (pentacene)_n grouped by the qualitative nature of the excited state: single-exciton (SE, or in other words the Frenkel exciton states as in eq 4); multiexciton (ME, meaning triplet-pair states); and CT states. For the two tetramers and the hexamer, these data represent the lower four states of each type. As system size increases, the CT states are stabilized more so than the SE and ME states.

= 0.3 bohr⁻¹ for LRC- ω PBE,⁸⁴ using the same data set. The same trend is observed in other π -conjugated systems when tuning according to the IE criterion of eq 13.⁹¹ It reflects the presence of 25% short-range Hartree–Fock exchange in ω PBEh that pushes out the length scale ($\sim\omega^{-1}$) on which the long-range Hartree–Fock exchange is required. Table S1 lists tuned values of ω for pentacene monomer that have been reported in various studies including the present one.

Since the tuned value of ω obtained for RSH- ω PBEh is smaller than that obtained for either RSH- ω PBE or RSH- μ BLYP (for which the tuned values of the range-separation

parameter are similar), one may expect qualitative differences when using RSH- ω PBEh in comparison to these other two functionals. To investigate this further, we applied the $J(\omega)$ tuning metric to larger clusters of pentacene, with tuned range-separation parameters listed in Table 2. The values decrease with increasing system size, which seems to be a general feature of the tuning procedure.^{68,91–93} Similar trends are observed for π -conjugated systems of increasing length,^{91,92} and for pentacene/C₆₀ clusters of increasing size.⁶⁸

The cluster-tuned values of ω provided in Table 2 are used for all subsequent calculations, meaning that calculations on different clusters use different values of the range-separation parameter, obtained individually via the $J(\omega)$ tuning procedure. In some sense, this means that we present a side-by-side comparison of results obtained using a (slightly) different functional for each cluster, although from another point of view we have made a consistent choice to set the frontier orbital energies according to the IE criterion of eq 13.

If the TDDFT calculations are repeated using a common value of ω for each cluster (e.g., the value obtained by tuning on the monomer), the resulting excitation energies are

Table 2. Tuned Range-Separation Parameters for Pentacene Clusters^a

system	ω (bohr ⁻¹)		
	RSH- ω PBE	RSH- μ BLYP	RSH- ω PBEh
dimer	0.170	0.175	0.135
tetramer (compact)	0.130	0.125	0.105
tetramer (linear)	0.150	0.145	0.115
hexamer	0.125		0.100

^aSame ω parameters tuned for OT-RSH functionals are used with the corresponding OT-sRSH functionals.

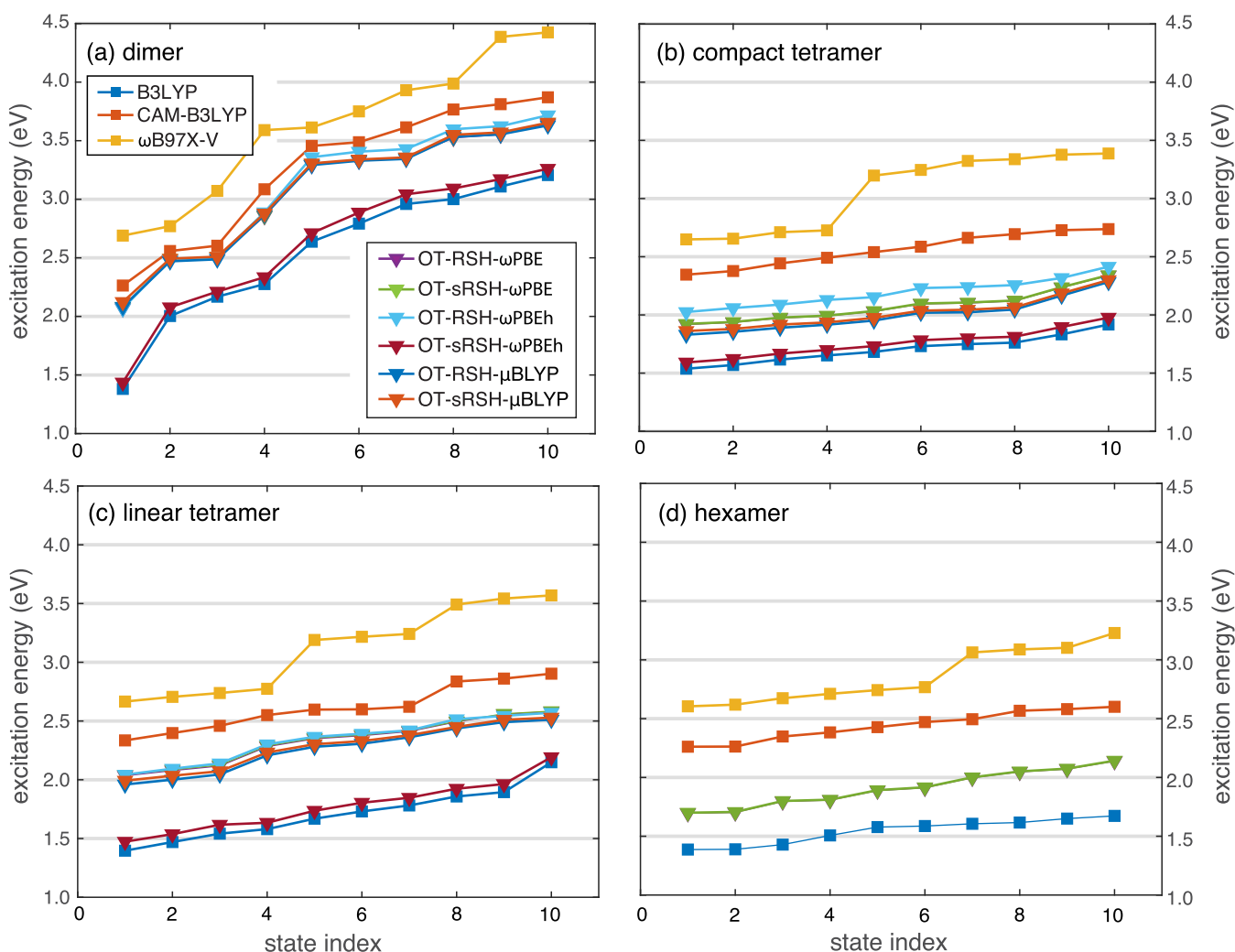


Figure 5. TDDFT excitation energies for clusters of pentacene: (a) dimer, (b) compact tetramer, (c) linear tetramer, and (d) hexamer. Results from optimally tuned (OT) range-separated hybrid (RSH) functionals as indicated by triangles, as are results from the corresponding “screened” (OT-sRSH) functionals. Results from three empirical functionals are indicated with squares. The OT-(s)RSH results are generally bounded above by the empirical RSH functionals CAM-B3LYP and ω B97X-V, and bounded below by B3LYP. The legend in panel a is applicable to all four panels but not all functionals were used in the hexamer case.

intermediate between those obtained using cluster-tuned values of ω and those obtained using the empirical CAM-B3LYP functional. As such, results using a common or averaged value of ω for all clusters will incur the same deficiencies as off-the-shelf functionals, defeating the purpose of the tuning procedure.

An unfortunate side effect of using a system-dependent tuning procedure is that it violates size consistency,⁹⁴ necessitating caution when computing binding energies and ground-state potential energy curves.⁹⁵ We expect this to be less of an issue for the calculations described here, which are aimed at investigating CT character in optical spectra. Size-consistency errors obtained using ω PBE are smaller than those obtained using some other RSH functionals,⁹⁵ and for prediction of CT excitation energies for molecules⁶⁴ and fundamental gaps for solids,⁶⁶ violation of size consistency may be considered an acceptable sacrifice to obtain reliable energetics at DFT cost. This requires that the frontier orbital energies be set correctly, and that cannot be accomplished (across a range of system sizes) using a common value of ω .

Excitation spectra for the four (pentacene)_n systems considered here, obtained using TDDFT, are plotted in Figure 5. For the first ten excited states (including some CT states), excitation energies predicted by the OT functionals are systematically lower than those predicted by CAM-B3LYP and ω B97X-V. Although the use of OT functionals to study CT states is well established at this point,^{64,69} to the best of our knowledge this disparity between OT- and conventional RSH functionals has not previously been noted in the studies of π -conjugated OPV materials. As noted in Section 1, most wave function studies of pentacene dimer have excluded the possibility of low-lying CT states.^{8,32,43,47,48} At least one prior TDDFT study on (pentacene)₄ also concluded that CT states appear only at energies above the Frenkel exciton states, and they are therefore inaccessible as intermediates in SF.⁴³

It is also worth noting that the energetics obtained using the empirical functionals vary more widely, e.g., comparing CAM-B3LYP and ω B97X-V results, whereas the spectra that emerge from the OT functionals are more consistent. This has been observed by others in a study of pentacene/C₆₀,⁶⁷ and suggests that IE tuning somewhat reduces the dependence of the

Table 3. Excitation Energies (ΔE , in eV) and Dipole Moments (μ , in D) of the Pentacene Dimer^a

state	ω B97X-V		CAM-B3LYP		OT-RSH- ω PBE		OT-sRSH- ω PBE		OT-RSH- ω PBEh		OT-sRSH- ω PBEh	
	ΔE	μ	ΔE	μ	ΔE	μ	ΔE	μ	ΔE	μ	ΔE	μ
0		1.20		1.18		1.18		1.16		1.22		1.21
1	2.69	2.16	2.26	12.91	2.07	14.97	2.08	15.11	2.07	14.80	1.44	18.40
2	2.77	1.21	2.56	1.19	2.48	1.70	2.49	1.67	2.48	1.53	2.08	13.37
3	3.07	12.70	2.60	0.93	2.50	1.68	2.51	1.68	2.50	1.63	2.21	1.96
4	3.59	1.10	3.09	17.00	2.86	16.17	2.86	16.28	2.89	16.38	2.34	7.55
5	3.61	1.30	3.46	0.81	3.29	8.97	3.30	7.75	3.36	9.63	2.71	13.21

^aStates identified as CT (according to μ) are highlighted in boldface type.

Table 4. Excitation Energies (ΔE , in eV) and Dipole Moments (μ , in D) of the Linear Pentacene Tetramer

state	ω B97X-V		CAM-B3LYP		OT-RSH- ω PBE		OT-sRSH- ω PBE		OT-RSH- ω PBEh		OT-sRSH- ω PBEh	
	ΔE	μ	ΔE	μ	ΔE	μ	ΔE	μ	ΔE	μ	ΔE	μ
0		3.78		3.72		3.72		3.67		3.87		3.84
1	2.67	2.94	2.34	4.41	2.03	11.20	2.04	11.39	2.04	11.04	1.47	21.03
2	2.71	3.26	2.40	6.00	2.08	12.12	2.09	12.21	2.09	11.95	1.54	21.35
3	2.74	3.50	2.46	4.58	2.12	10.65	2.12	10.76	2.14	10.33	1.62	27.96
4	2.77	3.91	2.55	3.99	2.28	11.37	2.29	11.51	2.30	9.77	1.63	28.17
5	3.19	13.92	2.60	2.54	2.35	10.02	2.35	10.07	2.37	8.52	1.74	20.23

excitation spectrum on the choice of functional, providing a more accurate description of the inherent electronic structure of the system itself. Crudely speaking, the IE criterion in eq 13 serves to eliminate self-interaction associated with the HOMO (and likely other frontier orbitals as well) to a significant extent. Excitation energies obtained using OT-RSH- ω PBE and OT-RSH- μ BLYP are similar and almost identical with their sRSH counterparts, whereas excitation energies computed using OT-RSH- versus OT-sRSH- ω PBEh are a bit different.

Let us now look at charge separation in these excited states. Roughly speaking, we might classify any state whose dipole moment μ is larger than the ground-state value as a “charge-separated” state, reserving the term “CT state” for states with very large dipole moments. (This distinction will be quite obvious from the data presented below, as there are a set of states for which $\mu > 10$ D.) Although some problems in assigning CT character based on dipole moment have been documented,^{25,38,96} especially for small clusters where states with artificially large or artificially small dipole moments can be obtained depending on whether the cluster breaks or preserves inversion symmetry, the static dipole moment remains a common parameter used to characterize charge separation.^{24,41,43} Here, we examine the dependence of the dipole moment on factors such as system size and level of theory. Both the excitation energies and the excited-state dipole moments obtained using OT-sRSH- μ BLYP are similar to those computed using OT-sRSH- ω PBE so only the latter values are discussed here. The OT-(s)RSH- μ BLYP results are provided in Table S2.

Dipole moments for the ground and excited states of pentacene dimer are listed in Table 3, computed using TDDFT with various functionals. (All excited-state dipole moments reported in this work are relaxed values.⁹⁷) We note that each functional predicts at least one CT state among the first five excited states. Whereas CAM-B3LYP and various OT-RSH functionals each predict that the very first state is a CT state, ω B97X-V does not. Hence we see stark differences in TDDFT predictions—among generally good-quality functionals—even for the first excited state of a dimer, which puts the sensitivity to functional firmly into focus. That the OT

functionals uniformly predict CT states demonstrates once again the consistency that emerges upon tuning, as observed already in the excitation spectra.

Next we consider the excited states computed for the linear tetramer (Table 4). For the dimer, the energetic ordering of the states depends upon the functional that is employed, but each functional predicts a state with $\mu > 12$ D in the low-energy spectrum. In contrast, for the linear tetramer we observe large differences in the degree of charge separation across different functionals. The ω B97X-V functional predicts the fifth excited state to be a CT state but no lower-lying states with large dipole moments are obtained, whereas CAM-B3LYP finds no state with a large dipole moment among the first five excited states. In contrast, the OT-RSH and OT-sRSH functionals predict that each of the first five excited states is a CT state, nearly all of them with $\mu > 10$ D as compared to ground-state dipole moments $\mu_0 < 4$ D. Moreover, none of these CT states stands out as having a much larger dipole moment than the others.

For this particular (pentacene)₄ cluster, the conclusion seems to be that low-energy CT states are obtained only with OT-RSH and OT-sRSH functionals. Note that this runs slightly counter to the scenario that was encountered in the early days of diagnosing CT problems in TDDFT calculations,⁶⁰ where semilocal functionals would predict a plethora of low-energy CT states at visible or ultraviolet wavelengths, many of which would be pushed to higher energies by global hybrid functionals and perhaps all of which would be absent when RSH functionals were used.^{60–62} The present results suggest that the low-energy CT states are not artifacts, but that they can be artificially pushed to higher energies by the addition of long-range Hartree–Fock exchange (in functionals such as CAM-B3LYP) if the frontier energy levels are not set carefully by means of IE tuning. Results for pentacene hexamer (Table S3) are consistent with these observations: although two moderately large dipole moments ($\mu_1 = 7.9$ D and $\mu_4 = 8.4$ D) are predicted using CAM-B3LYP (though none at all for ω B97X-V), these pale in comparison to dipole moments exceeding 15 D that are predicted for each of

Table 5. Excitation Energies (ΔE , in eV) and Dipole Moments (μ , in D) of the Compact Pentacene Tetramer

state	ω B97X-V		CAM-B3LYP		OT-RSH- ω PBE		OT-sRSH- ω PBE		OT-RSH- ω PBEh		OT-sRSH- ω PBEh	
	ΔE	μ	ΔE	μ	ΔE	μ	ΔE	μ	ΔE	μ	ΔE	μ
0		0.05		0.04		0.05		0.05		0.04		0.05
1	2.65	0.08	2.35	0.10	1.92	0.78	1.92	0.88	2.03	0.37	1.59	0.51
2	2.66	0.05	2.38	0.05	1.94	0.61	1.94	0.71	2.06	0.16	1.62	0.39
3	2.71	0.04	2.44	0.08	1.97	0.54	1.98	0.62	2.09	0.21	1.67	0.27
4	2.73	0.05	2.49	0.06	1.99	0.39	1.99	0.47	2.13	0.07	1.70	0.24
5	3.20	0.19	2.54	0.08	2.03	0.12	2.03	0.12	2.15	0.10	1.73	0.11

the first five excited states using OT-RSH- ω PBE and OT-sRSH- ω PBE.

It has been argued²⁵ that clusters lacking inversion symmetry may exhibit anomalously large dipole moments because they lack symmetrically situated monomers that might cancel the dipole moment through a superposition of forward and backward electron transfer. (Stated differently, a charge-resonance state such as that in eq 3 may have a much smaller dipole moment than either of the CT basis states from which it is formed.) It is therefore notable that we have applied the CAM-B3LYP and ω B97X-V functionals to precisely the same cluster geometries and obtained low-energy excited states that (for the most part) do not exhibit large dipole moments. Clearly, the sizable dipole moments predicted by OT-RSH functionals are not required by the geometries of these small, low-symmetry clusters, but instead they emerge specifically when these functionals are used.

The effect of cluster geometry is clearly evident in the results for the compact tetramer (Table 5), which are very different from those obtained for the linear tetramer (Table 4). In the former case, no CT states are observed among the first five excited states, regardless of the functional that is used, and all of the dipole moments are <1 D. Cluster geometry clearly has a significant effect on the particulars of the excitation spectrum in these small, finite clusters but this effect has not been clearly documented in previous studies, some of which are ambiguous about the details of the cluster geometries.^{42,43}

Examining results across all of the pentacene clusters considered here, we observe that excited-state dipole moments are not very different when comparing OT-RSH and OT-sRSH functionals, but they change considerably when the functional is a short-range hybrid, e.g., OT-RSH- ω PBEh. This behavior is seen consistently across all systems and mirrors trends in excitation energies, where various OT-RSH and OT-sRSH functionals predict very similar excitation energy profiles, but results from short-range hybrids are somewhat different; see Figure 5.

Most previous quantum chemistry studies on pentacene clusters have been carried out in vacuum, which facilitates straightforward comparison to the results presented above. In an attempt to mimic the effects of bulk dielectric stabilization and thus provide some indication whether our results for (pentacene)₆ are converged with respect to cluster size, we have recomputed excited states of this largest cluster in the presence of continuum boundary conditions. These calculations are performed with OT-sRSH- ω PBE using a nonequilibrium PCM formalism that is appropriate for vertical excitation energies.^{86–88} These calculations use a static dielectric constant $\epsilon_{st} = 3.6$ and an optical dielectric constant $\epsilon_{op} = 3.28$, and while one may reasonably argue that dielectric stabilization in a crystalline material should not have any orientational component at all, the ratio of the nonequilibrium

Pekar factor ($\epsilon_{op}^{-1} - \epsilon_{st}^{-1}$) to the equilibrium one ($1 - \epsilon_{st}^{-1}$) is ≈ 0.04 , suggesting that only 4% of the continuum reaction field is frozen upon vertical excitation.⁹⁸ The remaining 96% is polarized by the excited-state density, meaning that for these particular dielectric constants, the nonequilibrium PCM mostly simulates electronic reorganization, which is present even in crystalline environments.

Table 6 lists the excitation energies and dipole moments for the first five excited states of the hexamer, using both vacuum and PCM boundary conditions. Shifts in excitation energies engendered by the PCM are 0.04–0.08 eV, which we interpret as evidence that the use of OT-sRSH functionals combined with a hexamer cluster model is sufficient to capture most of the dielectric stabilization of the solid-state environment, such that the addition of PCM boundary conditions has little effect on the excitation energies. It has a major effect, however, on the dipole moments, which are much smaller in the PCM calculations than in the corresponding hexamer calculations under vacuum boundary conditions. This hints that the magnitude of the dipole moments documented above may be exaggerated in some cases by finite size effects. Nevertheless, several states with significant dipole moments remain in the PCM calculation, e.g., $\mu_2 = 5.9$ D and $\mu_3 = 13.4$ D.

Previous electronic structure calculations under periodic boundary conditions place the energy threshold for generating electron–hole pairs in bulk crystalline pentacene at 1.5–1.8 eV,^{35–38} with a low-energy optical spectrum that is dominated by CT-type excitations. In the present study, TDDFT excitation energies obtained for the hexamer (1.7–1.9 eV) are comparable to, or only slightly higher than, these previous calculations. Experimentally, the optical gap of pentacene thin films is found to be 1.7–1.8 eV,^{99–101} also consistent with these estimates. An oft-quoted value of 2.2 eV for the band gap^{102,103} represents the fundamental gap rather than the optical gap.³⁶

3.3. Electron–Hole Correlations. Finally, we examine charge separation in the TDDFT excited states using

Table 6. Excitation Energies (ΔE , in eV) and Dipole Moments (μ , in D) for Pentacene Hexamer.^a

state	vacuum		PCM ^b	
	ΔE	μ	ΔE	μ
0		2.66		1.88
1	1.70	16.15	1.74	0.57
2	1.71	15.74	1.79	5.90
3	1.80	17.45	1.73	13.37
4	1.81	16.71	1.81	2.92
5	1.89	15.12	1.82	9.75

^aOT-sRSH- ω PBE functional. ^bNonequilibrium ptSS + ptLR scheme of refs 86 and 87.

electron–hole correlation plots.⁵⁴ These come from the TDDFT transition densities $\gamma_{0k}(\mathbf{r}_h, \mathbf{r}_e)$, expressed here in terms of an electron coordinate \mathbf{r}_e and a hole coordinate \mathbf{r}_h . In previous studies of solid-state pentacene and other OPV materials, the correlation function

$$\mathcal{F}(\mathbf{r}) = \int |\gamma_{0k}(\mathbf{r}_h, \mathbf{r} + \mathbf{r}_h)|^2 d\mathbf{r}_h \quad (14)$$

has been used to infer information about charge separation in real space,^{38–40} but in an atom-centered basis set it is easy to separate $\gamma_{0k}(\mathbf{r}_h, \mathbf{r}_e)$ into localized contributions from individual atoms or fragments.¹⁰⁴ These are taken to be pentacene monomers in the present work, and one may define “CT numbers”

$$\Omega_{AB} = \int_A d\mathbf{r}_h \int_B d\mathbf{r}_e |\gamma_{0k}(\mathbf{r}_h, \mathbf{r}_e)|^2 \quad (15)$$

that quantify the amount of charge transfer from fragment A to fragment B.^{54,104} The values Ω_{AB} provide a compact representation of the correlated spatial (de)localization of the electron and the hole, revealing information that would be difficult to detect with orbital-based analyses alone, or with attachment/detachment or difference-density plots. If visualized in the form of a matrix Ω , for example, the CT numbers can distinguish between Frenkel exciton states and charge-resonance states. Both may be delocalized over multiple pentacene chromophores, but the Frenkel excitons are characterized by an electron and hole that occupy the same region of space, i.e., by amplitude along the diagonal, Ω_{AA} . A charge-resonance state, in contrast, consists of an electron and a hole that reside on different fragments and this manifests as significant off-diagonal elements of Ω . If the charge-resonance state is completely symmetric, in the sense of $|a_1| = |a_2|$ in eq 3, then the matrix Ω should be symmetric about its diagonal, but as the symmetry is broken and the charge-resonance state becomes an asymmetric CT state, this asymmetry will appear in Ω as well. Asymmetry in the Ω matrix therefore ought to be a signature of a state that is associated with a significant change in the dipole moment.

Figure 6 presents electron–hole correlation plots for the first four excited states of the compact tetramer, obtained with four different functionals. (Results for some additional functionals are presented in Figure S2.) Dipole moments for these excited states are listed in Table 5 and none exceeds 1 D, suggesting the absence of charge separation, yet the electron–hole correlations reveal that the qualitative nature of these states varies quite a bit from one functional to another. For example, each of the first four excited states obtained using ω B97X-V is characterized by a diagonally dominant Ω matrix, indicating Frenkel exciton states, whereas the OT-RSH and OT-sRSH functionals afford Ω matrices with mostly off-diagonal character, indicating charge separation. In the latter cases, however, Ω is essentially symmetric about the diagonal, consistent with charge-resonance character leading to a very small dipole moment. The CAM-B3LYP functional is an intermediate case, predicting a mixture of charge-resonance and Frenkel exciton character. These insights into the nature of the excited states reveal themselves immediately in the CT numbers Ω_{AB} but would have been difficult to obtain in other ways, suggesting that in studies of OPV materials (which invariably involve systems with multiple chromophores), relying on dipole moments or difference densities to infer charge-separated character is unreliable and may lead to

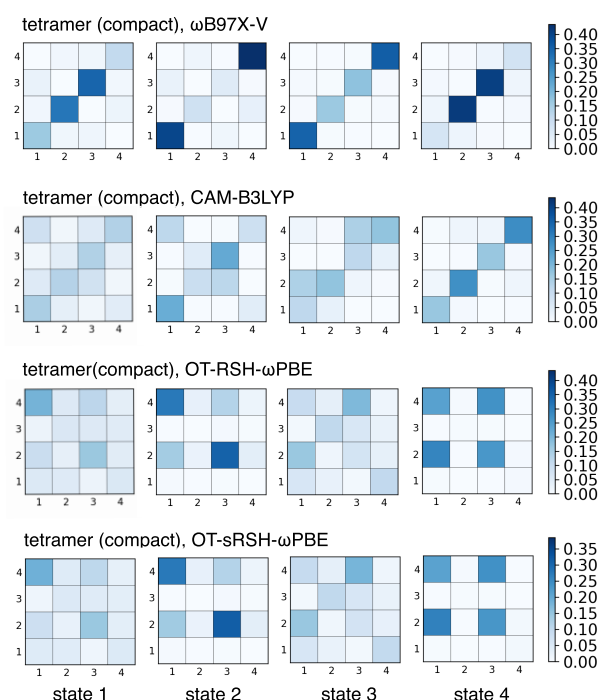


Figure 6. Electron–hole correlation plots for the first four excited states of the compact pentacene tetramer, obtained using four different functionals and presented in the form of matrices Ω , where Ω_{AB} is defined in eq 15.

incorrect conclusions regarding the nature of the states in question.

In contrast to the compact tetramer, the linear tetramer does exhibit excited states with very large dipole moments when OT-RSH functionals are used (see Table 4). The Ω matrices for these states (Figure 7) are consistent with this, with the OT-RSH- ω PBE and OT-sRSH- ω PBE functionals both exhibiting sizable off-diagonal CT numbers, which are moreover not symmetric as they were in the case of the compact structure of (pentacene)₄. Similar results are obtained using OT-(s)RSH- μ BLYP; see Figure S3. In contrast, these large off-diagonal Ω_{AB} elements are absent in the first four excited states predicted by ω B97X-V and CAM-B3LYP, and the corresponding dipole moments are much smaller as well.

The presence of a single prominent matrix element in the case of ω B97X-V shows that the absence of significant charge separation manifests here in a completely different way as compared to the compact structure of (pentacene)₄. In the linear structure, the low-lying states predicted by ω B97X-V are each localized on essentially just one chromophore, whereas in the compact structure these were Frenkel excitons delocalized over multiple pentacene monomers. In contrast, the OT-RSH and OT-sRSH functionals both suggest significant (albeit symmetric) charge-separation character for the compact tetramer and asymmetric CT character for the linear tetramer. Optimal tuning therefore makes a decisive difference in the underlying charge separation. Whereas OT-sRSH functionals are preferred over OT-RSH functionals for the calculation of fundamental gaps,^{71–73} both appear to behave in the same way when it comes to excitation energies and charge separation in these systems.

Figure 8 plots the Ω matrices for the pentacene hexamer and we note that CT excitations predicted by the OT-RSH and OT-sRSH functionals localize, to essentially a single inter-

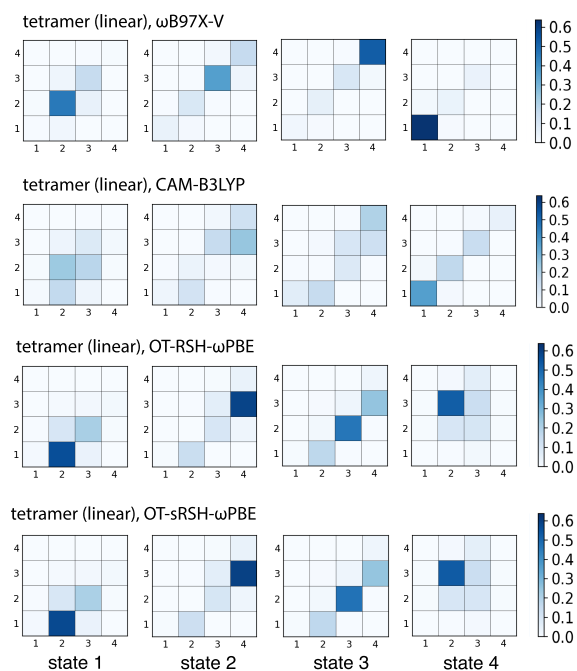


Figure 7. Electron–hole correlation plots for the first four excited states of the linear pentacene tetramer, obtained using four different functionals and presented in the form of matrices Ω , where Ω_{AB} is defined in eq 15.

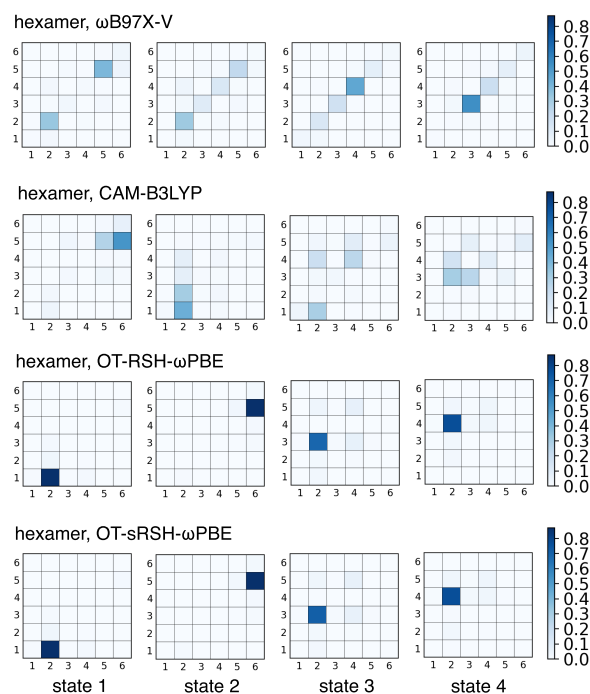


Figure 8. Electron–hole correlation plots for the first four excited states of the pentacene hexamer, obtained using four different functionals and presented in the form of matrices Ω , where Ω_{AB} is defined in eq 15.

molecular $A \rightarrow B$ electron transfer between neighboring fragments. The extent of CT is much more localized in the hexamer than it is (with the same functionals) in either tetramer structure. These states have significant dipole moments ($\mu > 15$ D, see Table S3), but it is not because

the CT length scale increases in this largest cluster. It actually decreases relative to that observed in either of the tetramer structures. This aberrant behavior with respect to cluster size suggests that these studies need to be pushed to larger clusters in order to examine converged results, and furthermore shows the danger in drawing general conclusions based on a quantum chemistry study of a single cluster size or a single cluster geometry.

4. CONCLUSIONS

We have used an *ab initio* exciton model to investigate the nature of low-lying excitations in pentacene clusters. This model is based on a direct-product “exciton-site basis” of diabatic states that includes locally-excited states, CT states, and triplet-pair ME states; coupling matrix elements between these states are computed from first principles. These calculations reveal low-energy CT states, even in pentacene dimer, which are substantially and preferentially stabilized as the system size increases. Although gas-phase quantum chemistry studies on pentacene (and tetracene) dimers generally find the CT states to be inaccessible at energies relevant to SF, our results indicate that the scenario changes as the model system is increased in size, mimicking the effects of dielectric stabilization in pentacene crystal or thin films.

We have also performed TDDFT calculations using optimally-tuned RSH and screened RSH functionals, in clusters ranging in size up to (pentacene)₆. Examining the degree of charge separation in the low-lying states, as evidenced by spatial correlations between electron and hole, we find that these optimally tuned functionals predict a larger degree of charge separation as compared to standard, empirically parametrized RSH functionals such as CAM-B3LYP and ω B97X-V. The nature of the low-lying states is thus sensitive to the nature of the functional, albeit in the opposite direction as compared to what is observed when spurious CT states (predicted by GGA functionals) are pushed to higher energies by global or range-separated hybrids.^{59–62} In the present case, the OT-RSH functionals predict CT states at lower energies as compared to CAM-B3LYP and ω B97X-V, suggesting the importance of tuning for establishing the frontier energy levels ϵ_{HOMO} and ϵ_{LUMO} .

Although the OT-RSH and OT-sRSH functionals do predict low-energy states with significant charge separation, these states are particularly sensitive not only to the nature of the functional but also to the size and geometry of the pentacene cluster. As such, these aspects of model design need to be considered more carefully than perhaps they have been in previous quantum chemistry studies. Our results using optimally-tuned functionals are consistent with predictions from periodic GW and Bethe–Salpeter calculations, in that there is significant charge separation in the low-lying excited states. As such, our results reconcile the long-standing discrepancy between these periodic calculations and various levels of quantum chemistry applied to dimers. These results suggest future studies ought to aim for extending the quantum chemistry studies to larger cluster sizes, in order to understand the optical spectra of these systems in greater detail.

■ ASSOCIATED CONTENT

Supporting Information

The Supporting Information is available free of charge at <https://pubs.acs.org/doi/10.1021/acs.jpcc.0c07932>.

Definitions of the functionals employed and additional TDDFT calculations (PDF)
Atomic coordinates (TXT)

AUTHOR INFORMATION

Corresponding Author

John M. Herbert – Department of Chemistry and Biochemistry, The Ohio State University, Columbus, Ohio 43210, United States; orcid.org/0000-0002-1663-2278; Email: herbert@chemistry.ohio-state.edu

Authors

Bushra Alam – Department of Chemistry and Biochemistry, The Ohio State University, Columbus, Ohio 43210, United States
Adrian F. Morrison – Department of Chemistry and Biochemistry, The Ohio State University, Columbus, Ohio 43210, United States

Complete contact information is available at:
<https://pubs.acs.org/10.1021/acs.jpcc.0c07932>

Notes

The authors declare the following competing financial interest(s): J.M.H. serves on the board of directors of Q-Chem Inc.

ACKNOWLEDGMENTS

This work was supported by the U.S. Department of Energy, Office of Basic Energy Sciences, Division of Chemical Sciences, Geosciences, and Biosciences under Award No. DE-SC0008550. Calculations were performed at the Ohio Supercomputer Center under Project No. PAA-0003.¹⁰⁵

REFERENCES

- (1) Smith, M. B.; Michl, J. Singlet fission. *Chem. Rev.* **2010**, *110*, 6891–6936.
- (2) Smith, M. B.; Michl, J. Recent advances in singlet fission. *Annu. Rev. Phys. Chem.* **2013**, *64*, 361–386.
- (3) Tayebjee, M. J. Y.; Gray-Weale, A. A.; Schmidt, T. W. Thermodynamic limit of exciton fission solar cell efficiency. *J. Phys. Chem. Lett.* **2012**, *3*, 2749–2754.
- (4) Tayebjee, M. J. Y.; McCamey, D. R.; Schmidt, T. W. Beyond Shockley–Queisser: Molecular approaches to high-efficiency photovoltaics. *J. Phys. Chem. Lett.* **2015**, *6*, 2367–2378.
- (5) Rao, A.; Friend, R. H. Harnessing singlet exciton fission to break the Shockley–Queisser limit. *Nat. Rev. Mater.* **2017**, *2*, 17063.
- (6) Chan, W.-L.; Berkelbach, T. C.; Provorse, M. R.; Monahan, N. R.; Tritsch, J. R.; Hybertsen, M. S.; Reichman, D. R.; Gao, J.; Zhu, X.-Y. The quantum coherent mechanism for singlet fission: Experiment and theory. *Acc. Chem. Res.* **2013**, *46*, 1321–1329.
- (7) Tamura, H.; Huix-Rotllant, M.; Burghardt, I.; Olivier, Y.; Beljonne, D. First-principles quantum dynamics of singlet fission: Coherent versus thermally activated mechanisms governed by molecular π stacking. *Phys. Rev. Lett.* **2015**, *115*, 107401.
- (8) Fuemmeler, E. C.; Sanders, S. N.; Pun, A. B.; Kumarasamy, E.; Zeng, T.; Miyata, K.; Steigerwald, M. L.; Zhu, X.-Y.; Sfeir, M. Y.; Campos, L. M.; Ananth, N. A direct mechanism of ultrafast intramolecular singlet fission in pentacene dimers. *ACS Cent. Sci.* **2016**, *2*, 316–324.
- (9) Japahuge, A.; Zeng, T. Theoretical studies of singlet fission: Searching for materials and exploring mechanisms. *ChemPlusChem* **2018**, *83*, 146–182.
- (10) Jones, A. C.; Kearns, N. M.; Ho, J.-J.; Flach, J. T.; Zanni, M. T. Impact of non-equilibrium molecular packings on singlet fission in microcrystals observed using 2D white-light microscopy. *Nat. Chem.* **2020**, *12*, 40–47.
- (11) Burgos, J.; Pope, M.; Swenberg, C. E.; Alfano, R. R. Heterofission in pentacene-doped tetracene single crystals. *Phys. Status Solidi B* **1977**, *83*, 249–256.
- (12) Sebastian, L.; Weiser, G.; Bäessler, H. Charge transfer transitions in solid tetracene and pentacene studied by electroabsorption. *Chem. Phys.* **1981**, *61*, 125–135.
- (13) Vaubel, G.; Baessler, H. Excitation spectrum of crystalline tetracene fluorescence: A probe for optically-induced singlet-exciton fission. *Mol. Cryst. Liq. Cryst.* **1971**, *15*, 15–25.
- (14) Thorsmølle, V. K.; Averitt, R. D.; Demsar, J.; Smith, D. L.; Tretiak, S.; Martin, R. L.; Chi, X.; Crone, B. K.; Ramirez, A. P.; Taylor, A. J. Morphology effectively controls singlet-triplet exciton relaxation and charge transport in organic semiconductors. *Phys. Rev. Lett.* **2009**, *102*, 017401.
- (15) Wilson, M. W. B.; Rao, A.; Johnson, K.; Gélinas, S.; di Pietro, R.; Clark, J.; Friend, R. H. Temperature-independent singlet exciton fission in tetracene. *J. Am. Chem. Soc.* **2013**, *135*, 16680–16688.
- (16) Tayebjee, M. J. Y.; Clady, R. G. C. R.; Schmidt, T. W. The exciton dynamics in tetracene thin films. *Phys. Chem. Chem. Phys.* **2013**, *15*, 14797–14805.
- (17) Morrison, A. F.; Herbert, J. M. Evidence for singlet fission driven by vibronic coherence in crystalline tetracene. *J. Phys. Chem. Lett.* **2017**, *8*, 1442–1448.
- (18) Dover, C. B.; Gallaher, J. K.; Frazer, L.; Tapping, P. C.; Petty, A. J., II; Crossley, M. J.; Anthony, J. E.; Kee, T. W.; Schmidt, T. W. Endothermic singlet fission is hindered by excimer formation. *Nat. Chem.* **2018**, *10*, 305–310.
- (19) Hetzer, C.; Guldi, D. M.; Tykwinski, R. R. Pentacene dimers as a critical tool for the investigation of intramolecular singlet fission. *Chem. - Eur. J.* **2018**, *24*, 8245–8257.
- (20) Beljonne, D.; Yamagata, H.; Brédas, J. L.; Spano, F. C.; Olivier, Y. Charge-transfer excitations steer the Davydov splitting and mediate singlet exciton fission in pentacene. *Phys. Rev. Lett.* **2013**, *110*, 226402.
- (21) Monahan, N.; Zhu, X.-Y. Charge transfer-mediated singlet fission. *Annu. Rev. Phys. Chem.* **2015**, *66*, 601–618.
- (22) Stern, H. L.; Cheminal, A.; Yost, S. R.; Broch, K.; Bayliss, S. L.; Chen, K.; Tabachnyk, M.; Thorley, K.; Greenham, N.; Hodgkiss, J. M.; Anthony, J.; Head-Gordon, M.; Musser, A. J.; Rao, A.; Friend, R. H. Vibronically coherent ultrafast triplet-pair formation and subsequent thermally activated dissociation control efficient endothermic singlet fission. *Nat. Chem.* **2017**, *9*, 1205–1212.
- (23) Casanova, D. Electronic structure study of singlet fission in tetracene derivatives. *J. Chem. Theory Comput.* **2014**, *10*, 324–334.
- (24) Basal, B. S.; Zirzmeier, J.; Hetzer, C.; Reddy, S. R.; Phelan, B. T.; Krzyaniak, M. D.; Volland, M. K.; Coto, P. B.; Young, R. M.; Clark, T.; Thoss, M.; Tykwinski, R. R.; Wasielewski, M. R.; Guldi, D. M. Evidence for charge-transfer mediation in the primary events of singlet fission in a weakly coupled pentacene dimer. *Chem.* **2018**, *4*, 1092–1111.
- (25) Berkelbach, T. C.; Hybertsen, M. S.; Reichman, D. R. Microscopic theory of singlet exciton fission. III. Crystalline pentacene. *J. Chem. Phys.* **2014**, *141*, 074705.
- (26) Mirjani, F.; Renaud, N.; Gorczak, N.; Grozema, F. C. Theoretical investigation of singlet fission in molecular dimers: The role of charge transfer states and quantum interference. *J. Phys. Chem. C* **2014**, *118*, 14192–14199.
- (27) Berkelbach, T. C.; Hybertsen, M. S.; Reichman, D. R. Microscopic theory of singlet exciton fission. II. Application to pentacene dimers and the role of superexchange. *J. Chem. Phys.* **2013**, *138*, 114103.
- (28) Yamagata, H.; Norton, J.; Hontz, E.; Olivier, Y.; Beljonne, D.; Brédas, J. L.; Silbey, R. J.; Spano, F. C. The nature of singlet excitons in oligoacene molecular crystals. *J. Chem. Phys.* **2011**, *134*, 204703.
- (29) Schuster, R.; Knupfer, M.; Berger, H. Exciton band structure of pentacene molecular solids: Breakdown of the Frenkel exciton model. *Phys. Rev. Lett.* **2007**, *98*, 037402.
- (30) Roth, F.; Schuster, R.; König, A.; Knupfer, M.; Berger, H. Momentum dependence of the excitons in pentacene. *J. Chem. Phys.* **2012**, *136*, 204708.

- (31) Casanova, D. Theoretical modeling of singlet fission. *Chem. Rev.* **2018**, *118*, 7164–7207.
- (32) Zimmerman, P. M.; Musgrave, C. B.; Head-Gordon, M. A correlated electron view of singlet fission. *Acc. Chem. Res.* **2013**, *46*, 1339–1347.
- (33) Kim, H.; Zimmerman, P. M. Coupled double triplet state in singlet fission. *Phys. Chem. Chem. Phys.* **2018**, *20*, 30083–30094.
- (34) Elliott, P.; Goldson, S.; Canahui, C.; Maitra, N. T. Perspective on double-excitations in TDDFT. *Chem. Phys.* **2011**, *391*, 110–119.
- (35) Tiago, M. L.; Northrup, J. E.; Louie, S. G. *Ab initio* calculation of the electronic and optical properties of solid pentacene. *Phys. Rev. B: Condens. Matter Mater. Phys.* **2003**, *67*, 115212.
- (36) Sharifzadeh, S.; Biller, A.; Kronik, L.; Neaton, J. B. Quasiparticle and optical spectroscopy of the organic semiconductors pentacene and PTCDA from first principles. *Phys. Rev. B: Condens. Matter Mater. Phys.* **2012**, *85*, 125307.
- (37) Cudazzo, P.; Gatti, M.; Rubio, A. Excitons in molecular crystals from first-principles many-body perturbation theory: Picene versus pentacene. *Phys. Rev. B: Condens. Matter Mater. Phys.* **2012**, *86*, 195307.
- (38) Sharifzadeh, S.; Darancet, P.; Kronik, L.; Neaton, J. B. Low-energy charge-transfer excitons in organic solids from first-principles: The case of pentacene. *J. Phys. Chem. Lett.* **2013**, *4*, 2197–2201.
- (39) Sharifzadeh, S.; Wong, C. Y.; Wu, H.; Cotts, B. L.; Kronik, L.; Ginsberg, N. S.; Neaton, J. B. Relating the physical structure and optoelectronic function of crystalline TIPS-pentacene. *Adv. Funct. Mater.* **2015**, *25*, 2038–2046.
- (40) Sharifzadeh, S. Many-body perturbation theory for understanding optical excitations in organic molecules and solids. *J. Phys.: Condens. Matter* **2018**, *30*, 153002.
- (41) Coto, P. B.; Sharifzadeh, S.; Neaton, J. B.; Thoss, M. Low-lying electronic excited states of pentacene oligomers: A comparative electronic structure study in the context of singlet fission. *J. Chem. Theory Comput.* **2015**, *11*, 147–156.
- (42) Zimmerman, P. M.; Zhang, Z.; Musgrave, C. B. Singlet fission in pentacene through multi-exciton quantum states. *Nat. Chem.* **2010**, *2*, 648–652.
- (43) Zimmerman, P. M.; Bell, F.; Casanova, D.; Head-Gordon, M. Mechanism for singlet fission in pentacene and tetracene: From single exciton to two triplets. *J. Am. Chem. Soc.* **2011**, *133*, 19944–19952.
- (44) Luzanov, A. V.; Casanova, D.; Feng, X.; Krylov, A. I. Quantifying charge resonance and multiexciton character in coupled chromophores by charge and spin cumulant analysis. *J. Chem. Phys.* **2015**, *142*, 224104.
- (45) Aguilar Suarez, L. E.; Kathir, R. K.; Siagri, E.; Havenith, R. W. A.; Faraji, S. Determination of electronic couplings in the singlet fission process using a nonorthogonal configuration interaction approach. *Adv. Quantum Chem.* **2019**, *79*, 263–287.
- (46) Mayhall, N. J.; Goldey, M.; Head-Gordon, M. A quasidegenerate second-order perturbation theory approximation to RAS-*n*SF for excited states and strong correlation. *J. Chem. Theory Comput.* **2014**, *10*, 589–599.
- (47) Feng, X.; Luzanov, A. V.; Krylov, A. I. Fission of entangled spins: An electronic structure perspective. *J. Phys. Chem. Lett.* **2013**, *4*, 3845–3852.
- (48) Zeng, T.; Hoffmann, R.; Ananth, N. The low-lying electronic states of pentacene and their roles in singlet fission. *J. Am. Chem. Soc.* **2014**, *136*, 5755–5764.
- (49) Morrison, A. F.; You, Z.-Q.; Herbert, J. M. *Ab initio* implementation of the Frenkel-Davydov exciton model: A naturally parallelizable approach to computing collective excitations in crystals and aggregates. *J. Chem. Theory Comput.* **2014**, *10*, 5366–5376.
- (50) Morrison, A. F.; Herbert, J. M. Low-scaling quantum chemistry approach to excited-state properties via an *ab initio* exciton model: Application to excitation energy transfer in a self-assembled nanotube. *J. Phys. Chem. Lett.* **2015**, *6*, 4390–4396.
- (51) Herbert, J. M.; Zhang, X.; Morrison, A. F.; Liu, J. Beyond time-dependent density functional theory using only single excitations: Methods for computational studies of excited states in complex systems. *Acc. Chem. Res.* **2016**, *49*, 931–941.
- (52) Morrison, A. F.; Herbert, J. M. Analytic derivative couplings and first-principles exciton/phonon coupling constants for an *ab initio* Frenkel-Davydov exciton model: Theory, implementation, and application to compute triplet exciton mobility parameters for crystalline tetracene. *J. Chem. Phys.* **2017**, *146*, 224110.
- (53) Shao, Y.; et al. Advances in molecular quantum chemistry contained in the Q-Chem 4 program package. *Mol. Phys.* **2015**, *113*, 184–215.
- (54) Plasser, F. TheoDORE A toolbox for a detailed and automated analysis of electronic excited state computations. *J. Chem. Phys.* **2020**, *152*, 084108.
- (55) Bardeen, C. J. The structure and dynamics of molecular excitons. *Annu. Rev. Phys. Chem.* **2014**, *65*, 127–148.
- (56) Yanai, T.; Tew, D. P.; Handy, N. C. A new hybrid exchange-correlation functional using the Coulomb-attenuating method (CAM-B3LYP). *Chem. Phys. Lett.* **2004**, *393*, 51–57.
- (57) Rohrdanz, M. A.; Herbert, J. M. Simultaneous benchmarking of ground- and excited-state properties with long-range-corrected density functional theory. *J. Chem. Phys.* **2008**, *129*, 034107.
- (58) Rohrdanz, M. A.; Martins, K. M.; Herbert, J. M. A long-range-corrected density functional that performs well for both ground-state properties and time-dependent density functional theory excitation energies, including charge-transfer excited states. *J. Chem. Phys.* **2009**, *130*, 054112.
- (59) Dreuw, A.; Weisman, J. L.; Head-Gordon, M. Long-range charge-transfer excited states in time-dependent density functional theory require non-local exchange. *J. Chem. Phys.* **2003**, *119*, 2943–2946.
- (60) Lange, A.; Herbert, J. M. Simple methods to reduce charge-transfer contamination in time-dependent density-functional calculations of clusters and liquids. *J. Chem. Theory Comput.* **2007**, *3*, 1680–1690.
- (61) Lange, A. W.; Rohrdanz, M. A.; Herbert, J. M. Charge-transfer excited states in a π -stacked adenine dimer, as predicted using long-range-corrected time-dependent density functional theory. *J. Phys. Chem. B* **2008**, *112*, 6304–6308. Lange, A. W.; Rohrdanz, M. A.; Herbert, J. M. Erratum: Charge-transfer excited states in a π -stacked adenine dimer, as predicted using long-range-corrected time-dependent density functional theory. *J. Phys. Chem. B* **2008**, *112*, 7345.
- (62) Isborn, C. M.; Mar, B. D.; Curchod, B. F. E.; Tavernelli, L.; Martinez, T. J. The charge transfer problem in density functional theory calculations of aqueously solvated molecules. *J. Phys. Chem. B* **2013**, *117*, 12189–12201.
- (63) Stein, T.; Kronik, L.; Baer, R. Reliable prediction of charge transfer excitations in molecular complexes using time-dependent density functional theory. *J. Am. Chem. Soc.* **2009**, *131*, 2818–2820.
- (64) Baer, R.; Livshits, E.; Salzner, U. Tuned range-separated hybrids in density functional theory. *Annu. Rev. Phys. Chem.* **2010**, *61*, 85–109.
- (65) Richard, R. M.; Herbert, J. M. Time-dependent density-functional description of the 1L_a state in polycyclic aromatic hydrocarbons: Charge-transfer character in disguise? *J. Chem. Theory Comput.* **2011**, *7*, 1296–1306.
- (66) Kronik, L.; Stein, T.; Refaely-Abramson, S.; Baer, R. Excitation gaps of finite-sized systems from optimally-tuned range-separated hybrid functionals. *J. Chem. Theory Comput.* **2012**, *8*, 1515–1531.
- (67) Zhang, C.-R.; Sears, J. S.; Yang, B.; Aziz, S. G.; Coropceanu, V.; Brédas, J.-L. Theoretical study of the local and charge-transfer excitations in model complexes of pentacene- C_{60} using tuned range-separated hybrid functionals. *J. Chem. Theory Comput.* **2014**, *10*, 2379–2388.
- (68) Yang, B.; Yi, Y.; Zhang, C.-R.; Aziz, S. G.; Coropceanu, V.; Brédas, J.-L. Impact of electron delocalization on the nature of the charge-transfer states in model pentacene/ C_{60} interfaces: A density functional theory study. *J. Phys. Chem. C* **2014**, *118*, 27648–27656.

- (69) Kümmel, S. Charge-transfer excitations: A challenge for time-dependent density functional theory that has been met. *Adv. Energy Mater.* **2017**, *7*, 1700440.
- (70) Kronik, L.; Kümmel, S. Dielectric screening meets optimally tuned density functionals. *Adv. Mater.* **2018**, *30*, 1706560.
- (71) Manna, A. K.; Refaely-Abramson, A.; Reilly, A. M.; Tkatchenko, A.; Neaton, J. B.; Kronik, L. Quantitative prediction of optical absorption in molecular solids from an optimally tuned screened range-separated hybrid functional. *J. Chem. Theory Comput.* **2018**, *14*, 2919–2929.
- (72) Bhandari, S.; Cheung, M. S.; Geva, E.; Kronik, L.; Dunietz, B. D. Fundamental gaps of condensed-phase organic semiconductors from single-molecule calculations using polarization-consistent optimally tuned screened range-separated hybrid functionals. *J. Chem. Theory Comput.* **2018**, *14*, 6287–6294.
- (73) Refaely-Abramson, S.; Sharifzadeh, S.; Jain, M.; Baer, R.; Neaton, J. B.; Kronik, L. Gap renormalization of molecular crystals from density-functional theory. *Phys. Rev. B: Condens. Matter Mater. Phys.* **2013**, *88*, 081204.
- (74) Mardirossian, N.; Head-Gordon, M. ω B97X-V: A 10-parameter, range-separated hybrid, generalized gradient approximation density functional with nonlocal correlation, designed by a survival-of-the-fittest strategy. *Phys. Chem. Chem. Phys.* **2014**, *16*, 9904–9924.
- (75) Mardirossian, N.; Head-Gordon, M. Thirty years of density functional theory in computational chemistry: An overview and extensive assessment of 200 density functionals. *Mol. Phys.* **2017**, *115*, 2315–2372.
- (76) Jacquemin, D.; Wathélet, V.; Perpète, E. A.; Adamo, C. Extensive TD-DFT benchmark: Singlet-excited states of organic molecules. *J. Chem. Theory Comput.* **2009**, *5*, 2420–2435.
- (77) Laurent, A. D.; Jacquemin, D. TD-DFT benchmarks: A review. *Int. J. Quantum Chem.* **2013**, *113*, 2019–2039.
- (78) Kim, J.; Hong, K.; Hwang, S.-Y.; Ryu, S.; Choi, S.; Kim, W. Y. Effects of the locality of a potential derived from hybrid density functionals on Kohn–Sham orbitals and excited states. *Phys. Chem. Chem. Phys.* **2017**, *19*, 10177–10186.
- (79) Refaely-Abramson, S.; Baer, R.; Kronik, L. Fundamental and excitation gaps in molecules of relevance for organic photovoltaics from an optimally tuned range-separated hybrid functional. *Phys. Rev. B: Condens. Matter Mater. Phys.* **2011**, *84*, 075144.
- (80) Refaely-Abramson, S.; Sharifzadeh, S.; Govind, N.; Autschbach, J.; Neaton, J. B.; Baer, R.; Kronik, L. Quasiparticle spectra from a nonempirical optimally tuned range-separated hybrid density functional. *Phys. Rev. Lett.* **2012**, *109*, 226405.
- (81) Refaely-Abramson, S.; Jain, M.; Sharifzadeh, S.; Neaton, J. B.; Kronik, L. Solid-state optical absorption from optimally tuned time-dependent range-separated hybrid density functional theory. *Phys. Rev. B: Condens. Matter Mater. Phys.* **2015**, *92*, 081204.
- (82) Sun, H.; Ryno, S.; Zhong, C.; Ravva, M. K.; Sun, Z.; Körzdörfer, T.; Brédas, J.-L. Ionization energies, electron affinities, and polarization energies of organic molecular crystals: Quantitative estimations from a polarizable continuum model (PCM)-tuned range-separated density functional approach. *J. Chem. Theory Comput.* **2016**, *12*, 2906–2916.
- (83) Perdew, J. P.; Levy, M. Comment on “Significance of the highest occupied Kohn–Sham eigenvalue. *Phys. Rev. B: Condens. Matter Mater. Phys.* **1997**, *56*, 16021–16028.
- (84) Lange, A. W.; Herbert, J. M. Both intra- and interstrand charge-transfer excited states in B-DNA are present at energies comparable to, or just above, the $^1\pi\pi^*$ excitonic bright states. *J. Am. Chem. Soc.* **2009**, *131*, 3913–3922.
- (85) Lange, A. W.; Herbert, J. M. A smooth, nonsingular, and faithful discretization scheme for polarizable continuum models: The switching/Gaussian approach. *J. Chem. Phys.* **2010**, *133*, 244111.
- (86) You, Z.-Q.; Mewes, J.-M.; Dreuw, A.; Herbert, J. M. Comparison of the Marcus and Pekar partitions in the context of non-equilibrium, polarizable-continuum reaction-field solvation models. *J. Chem. Phys.* **2015**, *143*, 204104.
- (87) Mewes, J.-M.; You, Z.-Q.; Wormit, M.; Kriesche, T.; Herbert, J. M.; Dreuw, A. Experimental benchmark data and systematic evaluation of two *a posteriori*, polarizable-continuum corrections for vertical excitation energies in solution. *J. Phys. Chem. A* **2015**, *119*, 5446–5464.
- (88) Mewes, J.-M.; Herbert, J. M.; Dreuw, A. On the accuracy of the state-specific polarizable continuum model for the description of correlated ground and excited states in solution. *Phys. Chem. Chem. Phys.* **2017**, *19*, 1644–1654.
- (89) Vydrov, O. A.; Scuseria, G. E. Assessment of a long-range corrected hybrid functional. *J. Chem. Phys.* **2006**, *125*, 234109.
- (90) Song, J.-W.; Hirose, T.; Tsuneda, T.; Hirao, K. Long-range corrected density functional calculations of chemical reactions: Redetermination of parameter. *J. Chem. Phys.* **2007**, *126*, 154105.
- (91) Körzdörfer, T.; Sears, J. S.; Sutton, C.; Brédas, J.-L. Long-range corrected hybrid functionals for π -conjugated systems: Dependence of the range-separation parameter on conjugation length. *J. Chem. Phys.* **2011**, *135*, 204107.
- (92) Bois, J.; Körzdörfer, T. Size-dependence of nonempirically tuned DFT starting points for G_0W_0 applied to π -conjugated molecular chains. *J. Chem. Theory Comput.* **2017**, *13*, 4962–4971.
- (93) Uhlig, F.; Herbert, J. M.; Coons, M. P.; Jungwirth, P. Optical spectroscopy of the bulk and interfacial hydrated electron from ab initio calculations. *J. Phys. Chem. A* **2014**, *118*, 7507–7515.
- (94) Livshits, E.; Baer, R. A well-tempered density functional theory of electrons in molecules. *Phys. Chem. Chem. Phys.* **2007**, *9*, 2932–2941.
- (95) Karolewski, A.; Kronik, L.; Kümmel, S. Using optimally tuned range separated hybrid functionals in ground-state calculations: Consequences and caveats. *J. Chem. Phys.* **2013**, *138*, 204115.
- (96) Petelenz, P.; Pac, B. Is dipole moment a valid descriptor of excited state’s charge-transfer character? *J. Am. Chem. Soc.* **2013**, *135*, 17379–17386.
- (97) Ronca, E.; Angeli, C.; Belpassi, L.; De Angelis, F.; Tarantelli, F.; Pastore, M. Density relaxation in time-dependent density functional theory: Combining relaxed density natural orbitals and multireference perturbation theories for an improved description of excited states. *J. Chem. Theory Comput.* **2014**, *10*, 4014–4024.
- (98) Cramer, C. J.; Truhlar, D. G. Implicit solvation models: Equilibria, structure, spectra, and dynamics. *Chem. Rev.* **1999**, *99*, 2161–2200.
- (99) Aoki-Matsumoto, T.; Furuta, K.; Yamada, T.; Moriya, H.; Mizuno, K.; Matsui, A. H. Excitonic photoluminescence in pentacene single crystal. *Int. J. Mod. Phys. B* **2001**, *15*, 3753–3756.
- (100) Park, S. P.; Kim, S. S.; Kim, J. H.; Whang, C. N.; Im, S. Optical and luminescence characteristics of thermally evaporated pentacene films on Si. *Appl. Phys. Lett.* **2002**, *80*, 2872–2874.
- (101) Faltermeier, D.; Gompf, B.; Dressel, M.; Tripathi, A. K.; Pflaum, J. Optical properties of pentacene thin films and single crystals. *Phys. Rev. B: Condens. Matter Mater. Phys.* **2006**, *74*, 125416.
- (102) Silinsh, E. A.; Belkind, A. I.; Balode, D. R.; Biseniece, A. J.; Grechov, V. V.; Taure, L. F.; Kurik, M. V.; Vertzymacha, J. I.; Bok, I. Photoelectrical properties, energy level spectra, and photogeneration mechanisms of pentacene. *Phys. Status Solidi A* **1974**, *25*, 339–347.
- (103) Silinsh, E. A.; Kolesnikov, V. A.; Muzikante, I. J.; Balode, D. R. On charge carrier photogeneration mechanisms in organic molecular crystals. *Phys. Status Solidi B* **1982**, *113*, 379–393.
- (104) Plasser, F.; Wormit, M.; Dreuw, A. New tools for the systematic analysis and visualization of electronic excitations. I. Formalism. *J. Chem. Phys.* **2014**, *141*, 024106.
- (105) Ohio Supercomputer Center, <http://osc.edu/ark:/19495/f5s1ph73>.